Manufacturing Letters xxx (xxxx) xxx

Contents lists available at ScienceDirect

Manufacturing Letters

journal homepage: www.elsevier.com/locate/mfglet

Letters

High-speed friction stir butt welding of 25.4 mm thick 7175-T79 aluminum alloy

Md. Reza-E-Rabby *, Hrishikesh Das, Tianhao Wang, Mageshwari Komarasamy, Scott A. Whalen, Glenn J. Grant

Applied Materials and Manufacturing Group, Pacific Northwest National Laboratory, 902 Battelle Boulevard, P.O. Box 999, MSIN K2-03, Richland, WA 99352, USA

A R T I C L E I N F O

Article history:
Received 8 May 2023
Received in revised form 30 June 2023
Accepted 1 August 2023
Available online xxxx

Keywords:
Friction stir welding (FSW)
High-speed welding
AA7175-T79
Single-sided FSW
Double-sided FSW

A B S T R A C T

This study presents the first experimental demonstration of high-speed friction stir butt welding of 25.4 mm thick AA7175-T79 aluminum alloy. The utilization of friction stir welding (FSW) tool pin threads that terminate away from the shoulder region reduced stress concentration during tool traversing. This tool design enabled a welding speed above 500 mm/min and a penetration depth greater than 10 mm without pin fracture near the shoulder. Two types of welds were performed: one-sided with full penetration and double-sided with partial penetration of the plate thickness. The junction of the double-sided friction stir welding (FSW) exhibited significant grain refinement (grain size 1.3 ± 0.8 μm) compared to other regions. Cross-weld tensile testing revealed high local strains at the double-sided FSW junction, which improved the yield strength by 20–24% compared to slower one-sided FSW. The joint efficiency of the as-welded, high-speed double-sided FSW was approximately 76% of the base material's ultimate tensile strength.

1. Introduction

Over the last 30 years, friction stir welding (FSW) [1] has become an established solid-state joining technique, especially for high-strength precipitate-strengthened aluminum (Al) alloys that are difficult to weld using conventional fusion-based techniques [2]. FSW of thick-section (greater than 25 mm) high-strength Al alloys at high welding speed (WS) is still challenging. Higher WS would expand applications of thick-section FSW in the industry since WS directly affects process productivity [3]. High-speed FSW of AA5XXX alloys [4,5] and AA6XXX alloys [5,6] has been reported with WS of 3000 mm/min for 2 mm thick AA5XXX and 1100 mm/min for 3 mm thick AA6XXX. In temperature-sensitive AA7XXX alloys, increasing WS would enhance the properties in the heat affected zone (HAZ) [7]. However, reports of increasing WS for FSW of greater than 25 mm thick AA7XXX alloys are scarce. The current reported ceiling speed of FSW decreases rapidly as workpiece thickness increases [see Fig. 1(a)] and most AA7XXX thicknesses in Fig. 1(a) are well below 12 mm [7–24]. Fig. 1(b-d) also compares reported FSW joint performance for many AA7XXX alloys. Reducing WS generally generates a higher peak temperature and a wider HAZ, which impairs mechanical performance since fracture occurs in the HAZ [25,26]. Therefore, enhancing WS of FSW on thick AA7XXX plates also would improve joint performance. This requires a tool design that (a) reduces in-plane forces, (b) expands process windows for AA7XXX (usually narrow); (c) operates below the machine force and torque capabilities; and (d) improves joint efficiency.

This work investigates joining AA7175 plates via FSW, which has structural application in riser pipes for ultradeep sea drilling (beyond 3000 m) [27]. Our goal was to increase the WS beyond reported values for any AA7XXX alloys greater than 25 mm thick and elucidate the effects of WS on joint performance. To that end, we demonstrated for the first time a maximum WS of 508 mm/min in double-sided welding of 25.4 mm thick AA7175 in a butt joint configuration. Further, measurements of grain size (GS) and hardness with different WS were complemented with tensile testing instrumented with digital image correlation (DIC).

2 . Materials and methods

FSW of two 25.4 mm thick AA7175-T79 plates was performed using FSW in a butt joint configuration. Three weld conditions were used to show the effects of WS on joint performance and GS distribution across the thickness. The tool pins, of lengths 25 mm (full penetration) and 13.7 mm (half penetration), had identical geometry. The thread on each pin is terminated such that

* Corresponding author.
E-mail address: md.reza-e-rabby@pnnl.gov (Md. Reza-E-Rabby).

https://doi.org/10.1016/j.mfglet.2023.08.140
2213-8463/

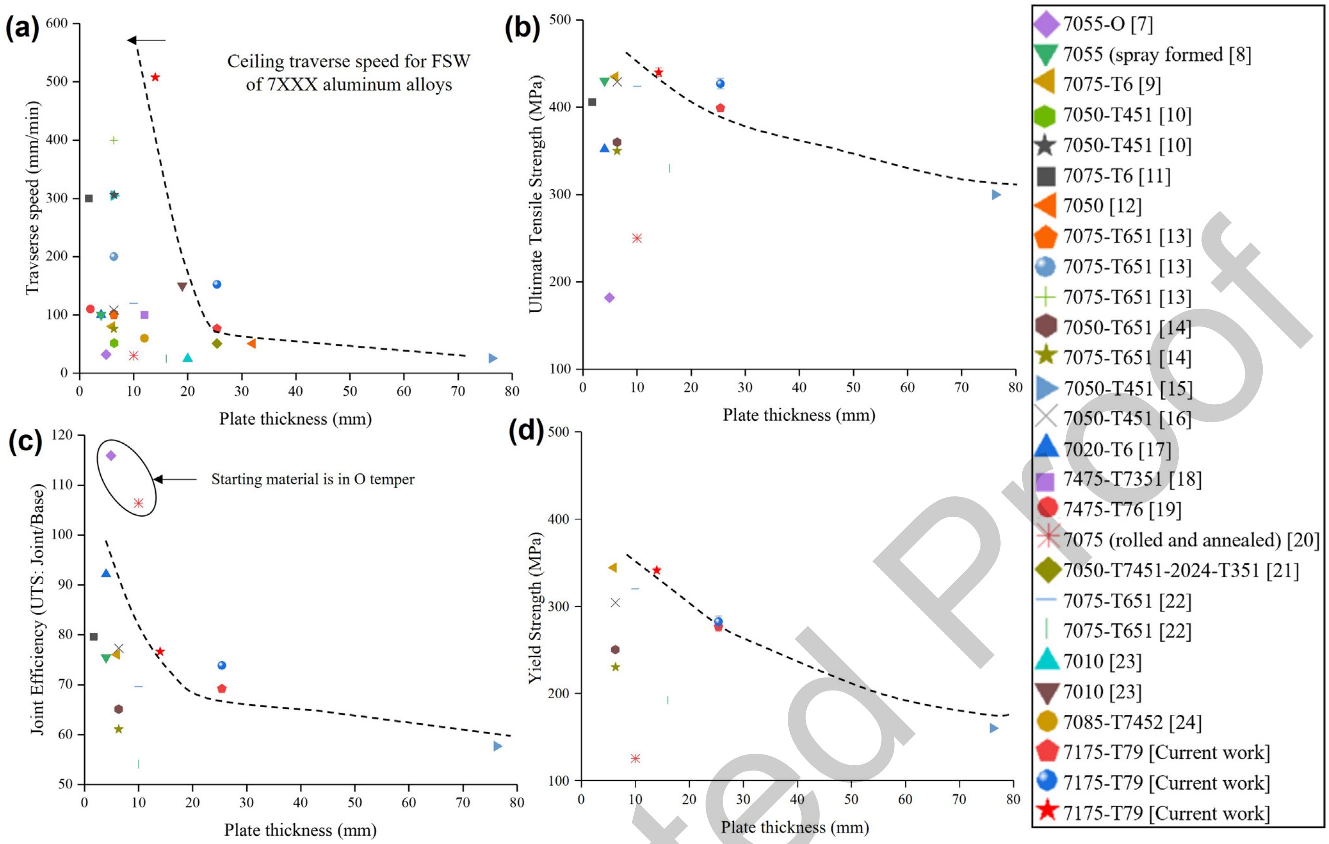

Fig. 1. (a) Traverse speed, (b) ultimate tensile strength, (c) joint efficiency, and (d) yield strength vs. plate thickness during FSW of AA7XXX aluminum alloys, and sources [7–24].

it leaves about 25% of the conical pin surface near the shoulder without thread (see Fig. 2). This tool design eliminates stress concentration at the thread root near the shoulder to prevent tools breaking at faster WS due to increased stress. Extreme plastic deformation under the tool shoulder diminishes the need for threading on the pin near this region. Supplemental Table S1 provides details about the tool dimensions, process control parameters, and response variables for three WS variations using two types of tools. All welding was performed with a 1.5° tilt angle. Specimens for weld cross-sectional investigation and tensile testing were extracted using an abrasive waterjet. Standard grinding and polishing sequences were followed to obtain metallographic samples for optical and scanning electron microscopy (SEM) and hardness mapping. Vickers microhardness mapping was conducted using a Clark CM-700AT indenter with 4.9 N for 12 s dwell time at 2.5 mm spacing in both the weld transverse and thickness directions. SEM was performed with a JEOL 7001 F microscope equipped with a Bruker e-Flash electron backscatter diffraction

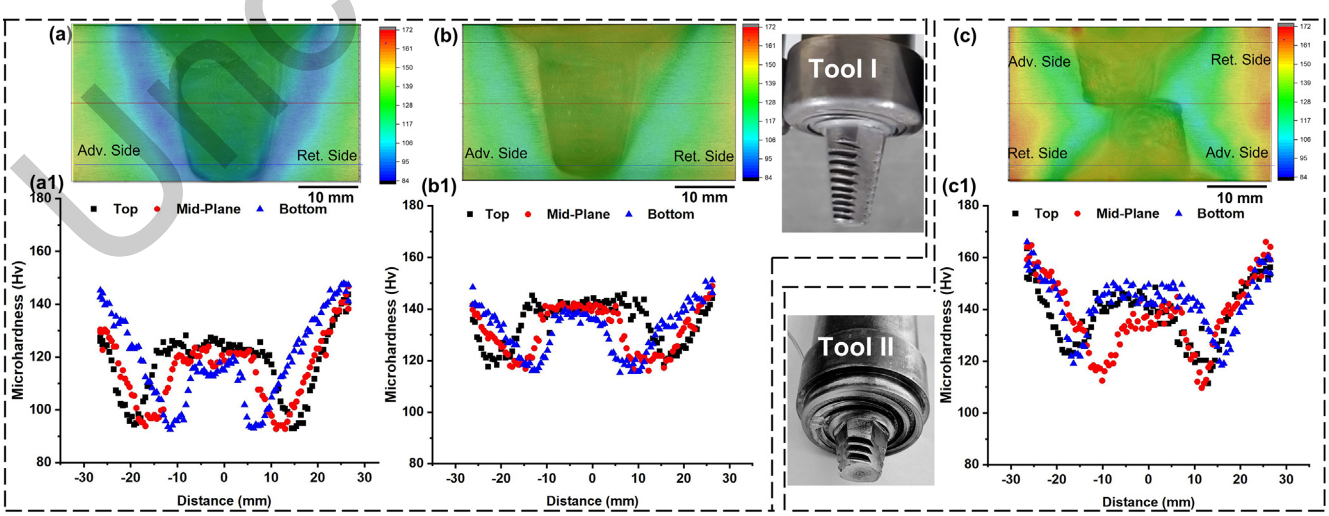

Fig. 2. Cross-sectional optical images overlaid with hardness maps; tool images; and hardness distributions of the single- and double-sided FSWs performed at WS of (a, a1) 76.2 mm/min, (b, b1) 152.4 mm/min, and (c, c1, c2) 508.0 mm/min.

(EBSD) detector. Cross-weld tensile testing instrumented with DIC was performed at room temperature on at least three specimens from each joining trial. Tensile testing was conducted per ASTM E8 at an extension rate of 2.54 mm/min using a 222 kN MTS test frame.

3 . Results and discussions

Optical microscopy images of weld cross sections overlaid with microhardness maps (color contours) for corresponding welding trials are shown in Fig. 2(a-c). Progressive contrast differences at the edges of the nugget zones (NZs) (etching differences from dark to light gray), which are often indicative of transition between the thermo-mechanically affected zone and part of the HAZ, were confirmed by the overlaid hardness maps in Fig. 2(a-c). While the microhardness maps show an overall pattern, the corresponding microhardness distributions (line plots) in Fig. 2(a1-c1) provide better insight. All three welds exhibit "W" shaped microhardness distributions typical for AA7XXX alloys, but the shape and pattern of the "W" contour is significantly different for each weld condition. The hardness distributions revealed that the average (arithmetic mean) minimum nugget and HAZ hardness for Weld B ($nugget_{avg.}$: 144 HV and avg. $HAZ_{min.}$: 123 HV) are considerably higher than those for A ($nugget_{avg.}$: 119 HV and avg. $HAZ_{min.}$: 97 HV). This overall softening in the NZ with a wider HAZ in A [Fig. 2(a1)] is attributed to precipitate coarsening from long thermal exposure at the lowest WS [7]. In Weld B [Fig. 2(b1)], the overall NZ and HAZ hardness increased significantly over those for A; this is expected, because doubling the WS increased the cooling rate. In Weld C, the $nugget_{avg.}$ and $HAZ_{min.}$ hardness increased to 147 HV and 119 HV, respectively [Fig. 2(c1)]. Higher WS in Weld C mitigated the substantial hardness reductions in both the NZ and HAZ seen in A and B because C had shorter thermal exposure. The mechanism and effects of thermal exposure on hardness distributions were previously reported [7,28–30].

Fig. 3(a-c) shows representative grain orientations via inverse pole figure (IPF) maps from the transverse sections for crown (a1, b1), midplane (a2, b2), and near-root (a3, c3) regions of single-pass FSW Trials A and B and first crown (c1), midplane (c2) and second crown (c3) regions for the double-pass Trial C. Recrystallization is observed in all the regimes, but the degrees of grain refinement are distinct across the weld thicknesses. In the IPF maps in Fig. 3, crown (~4 μm) and midplane (~3.2 μm) GSs are very similar for single-pass Welds A and B. In C, however, midplane GS is near submicron level (~1.3 μm) and ultrafine compared to those at the bottoms of plates in A and B. This is reasonable, because the EBSD map location for midplane C is the weld junction of first and second passes, with this highest WS producing more dynamic recrystallization, which correlates with faster cooling.

Fig. 4(a) shows engineering stress–strain curves for the base AA7175-T79 and the FSW butt joints at different WSs. The ultimate tensile strength (UTS) and 0.2% yield strength (YS) are also presented in the inset table of Fig. 3(a). The UTS of the high-speed (508 mm/min), double-pass Weld C was higher by 10% and 3%, respectively than for FSW at 76.2 mm/min (Weld A) and 152.4 mm/min (Weld B). Moreover, the YS of high-speed FSW increased about 21–24% over low and medium WS. The strain contour maps from DIC in Fig. 4(b) revealed initiation of localized yielding, consistent with the location of HAZ hardness minimum (comparing Fig. 2[a1-c1] and Fig. 4[b] A1, B1, and C1), and matched previous studies [31,32]. The DIC mapping of single-pass, low- and medium-speed FSW in Fig. 4(b) also revealed a subsequent high concentration of double necking strains (on advancing and retreating sides) before failure (A2 and B2) and after failure (A3 and B3) at the same locations. However, the high strain concentration (C2 in Fig. 4(b) in double-pass, high-speed FSW was near the overlapping interface of the two welds (at plate mid-depth) in the cross-link of double necking sites. The distribution of local plastic strain around this region impeded early necking, which might increase the YS. Consequently, the final failure (C3 in Fig. 4(b) occurred near the first-pass advancing / second-pass retreating side.

4. Conclusions

Novel FSW tool designs and double-sided welding of thick-section AA7175-T79 enabled weld speeds of 508 mm/min for depths up to 12 mm. The higher WS reduced thermal input into the HAZ, which in turn reduced coarsening and softening, and a

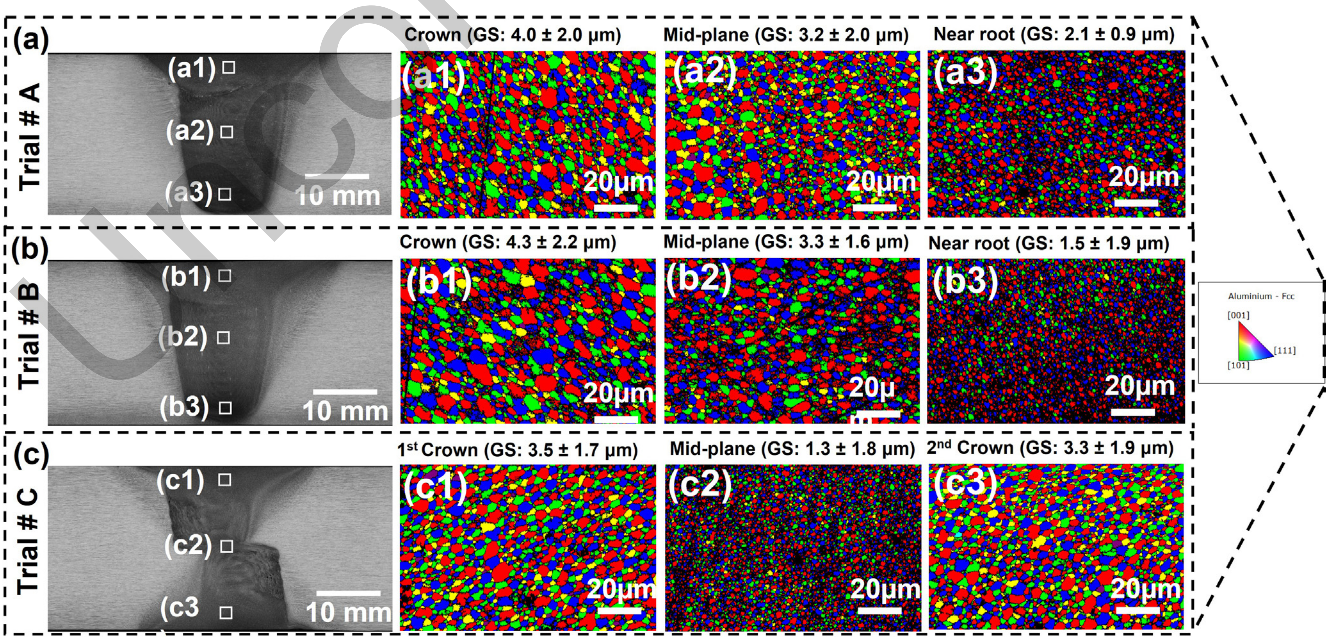

Fig. 3. Weld cross sections (left) and corresponding IPF maps at crown, midplane, and near-root for A (a1-a3) and B (b1-b3); at first crown, midplane, and second crown for C (c1-c3).

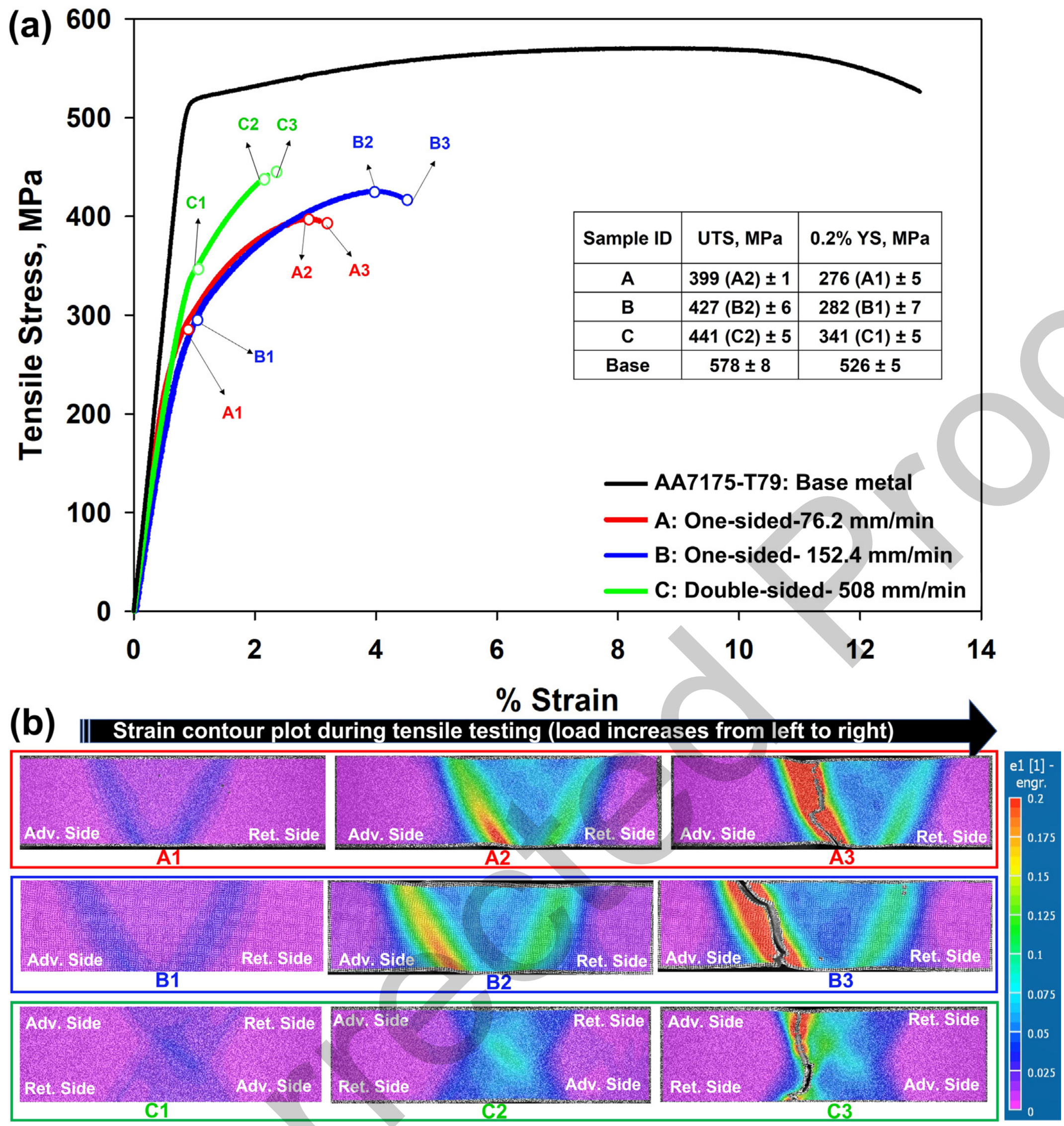

Fig. 4. (a) Engineering stress–strain curves of AA7175-T79 base material and after FSW at different welding speeds, (b) strain contour maps resulting from DIC showing (1) YS, (2) UTS before failure, and (3) UTS after failure.

joint efficiency of 76% was achieved. This study indicates that better joint performance and faster manufacturing throughput are possible for FSW thick-section 7XXX Al alloys.

Declaration of Competing Interest

The authors declare that they have no known competing financial interests or personal relationships that could have appeared to influence the work reported in this paper.

Acknowledgements

This research was funded by the Department of Energy (DOE) Office of Fossil Energy and Carbon Management under Field Work Proposal 71971. The authors acknowledge guidance and support from Roy Long and Dave Cercone of DOE's National Energy Technology Laboratory. Pacific Northwest National Laboratory is operated by Battelle Memorial Institute for the DOE under contract DE-AC05-76RL01830. The authors thank Anthony Guzman, Timothy Roosendaal, Nathan Canfield, and Angel Ortiz for their assistance in sample preparation and testing. Finally, the authors thank Mr. Douglas Waldron, President, Xymat, for his continuous support including providing the feedstock materials.

Appendix A. Supplementary material

Supplementary data to this article can be found online at https://doi.org/10.1016/j.mfglet.2023.08.140.

References

[1] Thomas WM, Nicholas ED, Needham JC, Murch MG, Temple-Smith P, Dawes CJ. Improvements relating to friction welding (friction stir welding and friction plunge welding). The Welding Institute, PCT World, Patent Number 0653265A2; 1993.
[2] Doshi SJ, Gohil A, Mehta N, Vaghasiya S. Challenges in Fusion Welding of Al alloy for Body in White. Mater Today-Proc 2018;5:6370–5. https://doi.org/10.1016/j.matpr.2017.12.247.
[3] Mononen J, Sirén M, Hänninen H. Cost comparison of FSW and MIG welded aluminium panels. Weld World 2003;47:32–5. https://doi.org/10.1007/BF03266406.
[4] Hovanski Y, Upadhyay P, Carsley J, Luzanski T, Carlson B, Eisenmenger M, et al. High-Speed Friction-Stir Welding to Enable Aluminum Tailor-Welded Blanks. J Miner, Met Mater Soc 2015;67:1045–53. https://doi.org/10.1007/s11837-015-1384-x.

[5] Rodrigues DM, Leitão C, Louro R, Gouveia H, Loureiro A. High speed friction stir welding of aluminium alloys. Sci Technol Weld Join 2010;15:676–81. https://doi.org/10.1179/136217110X12785889550181.

[6] Liu F, Fu L, Chen H. High speed friction stir welding of ultra-thin AA6061-T6 sheets using different backing plates. J Manuf Process 2018;33:219–27. https://doi.org/10.1016/j.jmapro.2018.05.020.

[7] Reynolds AP, Tang W, Khandkar Z, Khan JA, Lindner K. Relationships between weld parameters, hardness distribution and temperature history in alloy 7050 friction stir welds. Sci Technol Weld Join 2005;10:190–9. https://doi.org/10.1179/174329305X37024.

[8] Alali Alkhalaf A, Tesleva A, Polyakov P, Moschinger M, Fritsche S, Morozova I, et al. Modified Friction Stir Welding of Al–Zn–Mg–Cu Aluminum Alloy. In: Hovanski Y, Sato Y, Upadhyay P, Naumov AA, Kumar N, editors. Friction Stir Welding and Processing XI. Springer; 2021. p. 43–51.

[9] Canaday CT, Moore MA, Tang W, Reynolds AP. Through thickness property variations in a thick plate AA7050 friction stir welded joint. Mat Sci Eng a-Struct 2013;559:678–82. https://doi.org/10.1016/j.msea.2012.09.008.

[10] Dehghani K, Ghorbani R, Soltanipoor A. Microstructural evolution and mechanical properties during the friction stir welding of 7075-O aluminum alloy. Int J Adv Manuf Tech 2015;77:1671–9. https://doi.org/10.1007/s00170-014-6574-0.

[11] Feng AH, Chen DL, Ma ZY. Microstructure and cyclic deformation behavior of a friction-stir-welded 7075 Al alloy. Metall Mater Trans A 2010;41:957–71. https://doi.org/10.1007/s11661-009-0152-3.

[12] Fuller CB, Mahoney MW, Calabrese M, Micona L. Evolution of microstructure and mechanical properties in naturally aged 7050 and 7075 Al friction stir welds. Mat Sci Eng a-Struct 2010;527:2233–40. https://doi.org/10.1016/j.msea.2009.11.057.

[13] Golezani AS, Barenji RV, Heidarzadeh A, Pouraliakbar H. Elucidating of tool rotational speed in friction stir welding of 7020–T6 aluminum alloy. Int J Adv Manuf Tech 2015;81:1155–64. https://doi.org/10.1007/s00170-015-7252-6.

[14] Jata K, Sankaran K, Ruschau J. Friction-stir welding effects on microstructure and fatigue of aluminum alloy 7050–T7451. Metall Mater Trans A 2000;31:2181–92. https://doi.org/10.1007/s11661-000-0136-9.

[15] Komarasamy M, Alagarsamy K, Ely L, Mishra RS. Characterization of 3″through-thickness friction stir welded 7050–T7451 Al alloy. Mater Sci Eng A 2018;716:55–62. https://doi.org/10.1016/j.msea.2018.01.026.

[16] Lezaack MB, Simar A. Avoiding abnormal grain growth in thick 7XXX aluminium alloy friction stir welds during T6 post heat treatments. Mat Sci Eng a-Struct 2021;807:. https://doi.org/10.1016/j.msea.2021.140901140901.

[17] Linton VM, Ripley MI. Influence of time on residual stresses in friction stir welds in agehardenable 7xxx aluminium alloys. Acta Mater 2008;56:4319–27. https://doi.org/10.1016/j.actamat.2008.04.059.

[18] Magnusson L, Kallman L. Mechanical properties of friction stir welds in thin sheet of aluminium 2024, 6013 and 7475, Second international symposium on FSW, Gothenburg, Sweden, 2000, pp. 1555–1620.

[19] Mao Y, Ke L, Liu F, Liu Q, Huang C, Xing L. Effect of tool pin eccentricity on microstructure and mechanical properties in friction stir welded 7075 aluminum alloy thick plate. Mater Design 2014;62:334–43. https://doi.org/10.1016/j.matdes.2014.05.038.

[20] Prime MB, Gnäupel-Herold T, Baumann JA, Lederich RJ, Bowden DM, Sebring RJ. Residual stress measurements in a thick, dissimilar aluminum alloy friction stir weld. Acta Mater 2006;54:4013–21. https://doi.org/10.1016/j.actamat.2006.04.034.

[21] Rao TS, Reddy GM, Rao SK. Microstructure and mechanical properties of friction stir welded AA7075–T651 aluminum alloy thick plates. T Nonferr Metal Soc 2015;25:1770–8. https://doi.org/10.1016/S1003-6326(15)63782-7.

[22] Sullivan A, Derry C, Robson JD, Horsfall I, Prangnell PB. Microstructure simulation and ballistic behaviour of weld zones in friction stir welds in high strength aluminium 7xxx plate. Mater Sci Eng A 2011;528:3409–22. https://doi.org/10.1016/j.msea.2011.01.019.

[23] Xu WF, Luo YX, Fu MW. Microstructure evolution in the conventional single side and bobbin tool friction stir welding of thick rolled 7085–T7452 aluminum alloy. Mater Charact 2018;138:48–55. https://doi.org/10.1016/j.matchar.2018.01.051.

[24] Zhao Y, Wang Q, Chen H, Yan K. Microstructure and mechanical properties of spray formed 7055 aluminum alloy by underwater friction stir welding. Mater Design 2014;56:725–30. https://doi.org/10.1016/j.matdes.2013.11.071.

[25] Mishra RS, Komarasamy M. Friction stir welding of high strength 7XXX aluminum alloys. 1st ed. Butterworth-Heinemann; 2016.

[26] Sheikh-Ahmad J, Ozturk F, Jarrar F, Evis Z. Thermal history and microstructure during friction stir welding of Al–Mg alloy. Int J Adv Manuf Technol 2016;86:1071–81. https://doi.org/10.1007/s00170-015-8239-z.

[27] Gelfgat M, Chizhikov V, Kolesov S, Alkhimenko A, Shaposhnikov V. Application of Aluminum Alloy Tube Semis: Problems and Solutions in the Development of Exploration, Production and Transportation Business of Hydrocarbons in the Arctic, SPE Arctic and Extreme Environments Technical Conference and Exhibition, OnePetro, Moscow, Russia, 2013.

[28] Hassan KA, Prangnell P, Norman A, Price D, Williams S. Effect of welding parameters on nugget zone microstructure and properties in high strength aluminium alloy friction stir welds. Sci Technol Weld Joi 2003;8:257–68. https://doi.org/10.1179/136217103225005480.

[29] Kamp N, Sullivan A, Tomasi R, Robson J. Modelling of heterogeneous precipitate distribution evolution during friction stir welding process. Acta Mater 2006;54:2003–14. https://doi.org/10.1016/j.actamat.2005.12.024.

[30] Sullivan A, Robson J. Microstructural properties of friction stir welded and post-weld heat-treated 7449 aluminium alloy thick plate. Mater Sci Eng A 2008;478:351–60. https://doi.org/10.1016/j.msea.2007.06.025.

[31] Threadgill PL, Leonard AJ, Shercliff HR, Withers PJ. Friction stir welding of aluminium alloys. Int Mater Rev 2009;54:49–93. https://doi.org/10.1179/174328009X411136.

[32] Wu H, Chen Y-C, Strong D, Prangnell P. Stationary shoulder FSW for joining high strength aluminum alloys. J Mater Process Tech 2015;221:187–96. https://doi.org/10.1016/j.jmatprotec.2015.02.015.